

Investigation of the effect of rapidly solidified braze ribbons on the microstructure of brazed joints

K Bobzin¹, M Öte¹, S Wiesner¹, P Rochala¹, J Mayer², A Aretz², R Iskandar² and A Schwedt²

¹Surface Engineering Institute, RWTH Aachen University, Kackertstraße 15, 52056 Aachen, Germany

²Central Facility for Electron Microscopy, RWTH Aachen University, Ahornstraße 55, 52074 Aachen, Germany

Abstract. Shrinkage and warpage due to melting and solidification are crucial for the geometric precision of related components. In order to assure a high geometric precision, the formation of the microstructure in the joint during brazing must be taken into consideration. An extensive interaction can occur between liquid melt and base material, resulting in the formation of distinctive phases. This interaction depends on the parameters of the brazing process. However, the consequences of the interaction between phase formation and process parameters in terms of geometric precision cannot be estimated yet. Insufficient quality of the joint can be a result. In this study, investigations focus on the process of solidification in terms of time dependent diffusion behavior of elements. Therefore, microcrystalline and amorphous braze ribbons based on Ti are produced by rapid solidification and are used for joining. The microstructure of the braze ribbons as well as the melting behavior and phase formation during brazing are considered to be of particular importance for the mechanical properties of the brazed components.

1. Introduction

Brazing is defined as a joining process using a molten filler metal that has a liquidus temperature lower than the solidus temperature of the base material. During the brazing process, the liquid filler metal is drawn into the gap between the parts to be joined and solidifies during cooling. As a result, a firm bonding between the parts is established. Diffusion processes between filler metal and base material play an important role during the brazing process [1]. Numerous factors, such as the process parameters during brazing, the properties of substrate and brazing material, as well as the geometry of the components have an impact on the process of melting and solidification. The interaction of these factors can lead to the formation of an uncontrollable microstructure of the joint with various properties. It is hardly possible to affect or to control the above-mentioned factors during the brazing process. As a result, shrinkage, misalignment and warpage can occur resulting in rejected parts during quality control. For base materials with defined microstructure and tailored properties, there is also the risk of altering the material's microstructure during the brazing process due to the heat treatment in the heat affected zone. Thus, the base material is meant to be thermally stressed as few as possible during brazing. An interdisciplinary research group of RWTH Aachen University (SFB 1120) targets on producing brazed joints with high geometric precision by controlling and affecting the factors that have impact on the final joint properties.



During brazing, a molten liquid phase, characterized by intrinsic melt dynamics, is formed in the braze gap and solidifies subsequently. Boundary conditions of the braze process, such as irregular cooling due to inhomogeneous transport of energy, different thermal expansion coefficients of base material and braze material, non-uniform volume contraction or the formation of unwanted phases in the braze gap can affect the geometric precision of the brazed joint and can lead to joint flaws like pores or stress cracking. As these effects depend on multiple factors such as material, process parameters and component geometry, every single braze joint must be considered as an individual issue in terms of process design, when high precision in production shall be reached.

The complex metallurgical processes between filler metal and base material are yet to be fully understood and subject to intensive researches. For this reason, it is necessary to identify, analyze and understand precision-relevant factors in brazing in order to control them and manufacture high-precision components. Therefore, an increased repeatability of the process zone that is formed by braze material and heat influenced zone in the substrate is needed. Phase composition, thermal properties and remelting temperature of joints have to be investigated in order to understand the mechanisms that lead to geometric flaws during brazing and to prevent the substrate from altering its tailored properties during the brazing process.

In this work, Ti-based braze ribbons are produced by melt spinning (MS) and used for brazing. Melt spinning is a process to produce thin metallic ribbons from a molten liquid by rapid cooling, with cooling rates up to $\dot{T} = 10^6$ K/s. The braze ribbons can thus solidify in amorphous, semicrystalline or fully crystalline state. According to the objectives mentioned above, these braze ribbons are analysed in terms of their initial microstructure and material properties. Additional joining experiments with a hot-working steel enable the time- and temperature-resolved analysis of bonds, as well as the determination of the process parameters that affect the geometric precision. The aim of the investigations is thus to design brazing processes that allow to manufacture high-quality joints with high geometric precision.

2. Materials

For filler metal development, the production of corrosion-resistant brazed joints with high toughness was the primary target. Additionally, the filler metal should be processable via melt spinning, producing flexible ribbons. Furthermore, it should be possible to use it for joining the hot-working steel with the material number 1.2343. This steel is commonly used in tool construction. It is characterized by high heat resistance, high toughness and good thermal conductivity. Thus, this steel is very well suited for tools for injection moulding or permanent mould casting. The composition of the steel is shown in table 1.

Table 1. Metallurgical composition of the hot-working steel 1.2343.

1.2343	C	Si	Mn	Cr	Mo	V	Fe
[wt.-%]	0.38	1.00	0.40	5.30	1.20	0.40	91.32

The hot-working steel's austenitization temperature is $T_{a/\gamma} = 1,030$ °C. Since the phase transformation of this material has to be avoided during brazing, a potential filler metal has to have a melting temperature $T_m < T_{a/\gamma}$. As starting point for the filler metal development, the alloy Ti70Ni30 with the composition of $m_{Ti} = 70$ wt.-% Ti and $m_{Ni} = 30$ wt.-% Ni was used. According to the corresponding binary phase diagram, the liquidus temperature amounts to $T_{liq} = 942$ °C. In this study, an alloy was sought with a lower liquidus temperature and more favorable properties. As a result, the alloy Ti67Cu15Ni15Si3 was developed.

3. Experiments

In this section, the melt spinning process used to produce the braze ribbons is presented as well as the high vacuum brazing process. Modern techniques for characterizing ribbons and joints on an atomic level are used, including scanning electron microscopy (SEM), transmission electron microscopy (TEM) and light microscopy. Additionally, differential scanning calorimetry (DSC) measurements for analyzing the thermal properties of the braze ribbons are conducted. Finally, the hardness testing method for investigating the mechanical properties of the joints is presented.

3.1 Melt Spinning Process

All the braze ribbons used in this work are produced by melt spinning. The Melt Spinner SC, manufactured by Edmund Bühler GmbH, Hechingen, Germany, was used for ribbon production. The basic set-up of such a system is shown in figure 1.

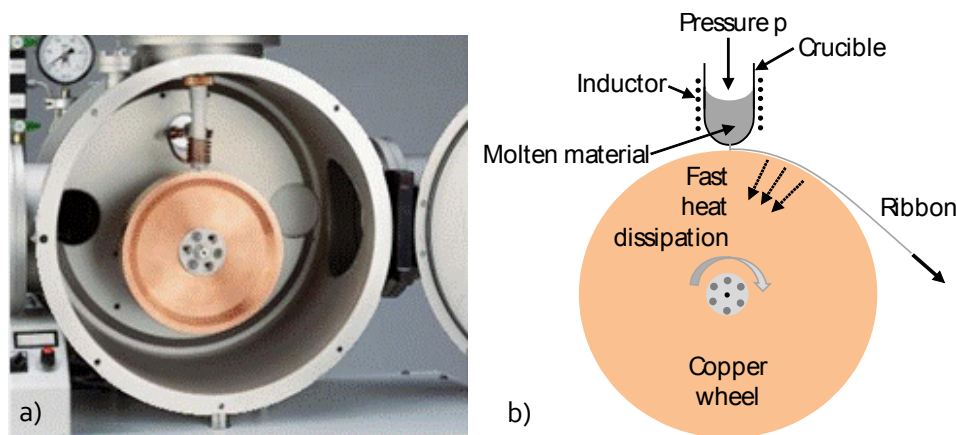


Figure 1. a) Recipient of the Melt Spinner SC with copper roll, induction coil and crucible. [2] b) Schematic of a melt spinning system.

For ribbon production, the components of the alloy are prealloyed in an arc furnace. Subsequently, the pre-alloyed material is melted inductively under argon atmosphere in the crucible. After the melt is homogenized, it is ejected from the crucible by protective gas pressure and hits a rotating, water-cooled copper roll. The melt cools down with a cooling rate up to $\dot{T} = 10^6$ K/s by rapid heat dissipation, due to the large contact area with the cooled roll. The rotational velocity of the roll correlates with the cooling rate of the melt [3, 4]. By controlling the rotational velocity, an amorphous, semi-crystalline or fully crystalline microstructure can be generated in the ribbon. In general, high cooling rates suppress the formation of a crystalline structure [5]. Besides the rotational velocity of the copper roll, the pressure during ejection also has a great impact on the formation of microstructure in the braze ribbon. After the ejection of the melt, the ribbon is carried along with the roll and a fully solidified ribbon is released from it due to the centrifugal force [3].

In this work, braze ribbons were produced by melting the alloy in a quartz crucible with a nozzle. The slit of the nozzle was $s = 5$ mm in width and $d = 0.4$ mm in thickness. The distance between copper wheel and slit nozzle was $h = 0.5$ mm and the rotational velocity of the roll was $f = 25$ Hz. For the alloy Ti70Ni30 the eject temperature was $T_{\text{eject}} = 1,100$ °C. For Ti67Cu15Ni15Si3 $T_{\text{eject}} = 1,200$ °C was chosen. For all experiments, the ejection pressure was $p = 300$ mbar.

3.2 Transmission Electron Microscopy (TEM)

Transmission electron microscopy, a special operating mode of electron microscopy, allows to investigate the lattice structure of a metallic sample. Microstructures down to the atomic level can be depicted and analyzed, as well as phase conditions, microstructural compositions, segregations, diffusion zones, grain boundaries and crystallographic defects such as dislocations or stacking faults.

For TEM analysis in this work, lamellae of the Ti70Ni30 and Ti67Cu15Ni15Si3 braze ribbons were prepared by using the focused ion beam (FIB) FIB Strata 205 by FEI, Hillsboro, USA. To allow electrons to fully permeate the samples, they are not allowed to have more than $d = 300$ nm in thickness. The investigations were carried out using STEM-HAADF mode (scanning transmission electron microscopy – high-angle annular dark field) of a Zeiss LIBRA 200 FE microscope by Carl Zeiss AG Microscopy, Oberkochen, Germany. Aim of the investigations was to detect the amorphous or crystalline structure of the braze ribbons.

3.3 Differential Scanning Calorimetry (DSC)

Differential scanning calorimetry is a thermal analysis method for measuring heat flows into a sample while heating or cooling the sample in a defined temperature program. With this method, investigations on phase transitions, chemical reactions or sintering reactions can be conducted. Furthermore, thermodynamic material properties, such as the specific heat capacity, can be determined. [6, 7] In the present work, the DSC system Setsys Evolution from Setaram Instrumentation AG, Caluire, France, was used to analyze the Ti70Ni30 and Ti67Cu15Ni15Si3 braze ribbons. Investigations targeted on the determination of temperatures for phase transitions, recrystallization and melting. Heating and cooling rates were chosen to be $\dot{T} = 10$ K/min. All investigations were conducted in argon atmosphere.

3.4 Process of brazing

For brazing experiments, the furnace MOV 553T from PVA TePla AG, Wettenberg, Germany, was used. Brazing experiments were conducted with the Ti70Ni30 and Ti67Cu15Ni15Si3 braze ribbons as well as the steel 1.2343. Braze joints were produced, applying a static pressure of $p = 5.3$ N/mm² on the sandwich construction during brazing. All brazing experiments were conducted in high vacuum. In a first step, the samples were heated to $T = 860$ °C with a heating rate of $\dot{T} = 20$ K/min. This temperature was maintained for $t = 10$ min. Subsequently, further heating was carried out up to the brazing temperature of $T_{\text{brazing}} = 1,010$ °C with a heating rate of $\dot{T} = 10$ K/min. At this temperature, the samples were brazed for $t = 30$ min. Finally, the samples were cooled with a cooling rate of $\dot{T} = 32$ K/min until room temperature was reached.

3.5 Hardness testing

For micro-hardness testing, cross sections of the braze joints, according to chapter 3.4, were prepared. Measurements were conducted, using the Fischerscope HM 2000 by Helmut Fischer GmbH, Sindelfingen, Germany. A maximum load of $F = 500$ mN was chosen. The maximum depth of indentation of the testing pyramid was $h = 5$ µm.

4. Results and discussion

In this section the results of the analysis of the braze ribbons and the braze joints are presented and discussed. In addition, relations between braze ribbon properties, substrate and braze joint are sought, discussed and evaluated with regard to precision-relevant aspects.

4.1 Melt Spinning Prozess

Starting from the alloy Ti70Ni30, Cu was added in order to suppress the formation of intermetallic phases during the brazing process. Furthermore, Si was added to the alloy for lowering its melting temperature and for increasing the alloy's diffusional activity [8]. As a result, the alloy Ti67Cu15Ni15Si3 was developed. Both Ti-based alloys could successfully be processed in the melt spinning process, obtaining braze ribbons with uniform thickness and width, figure 2.

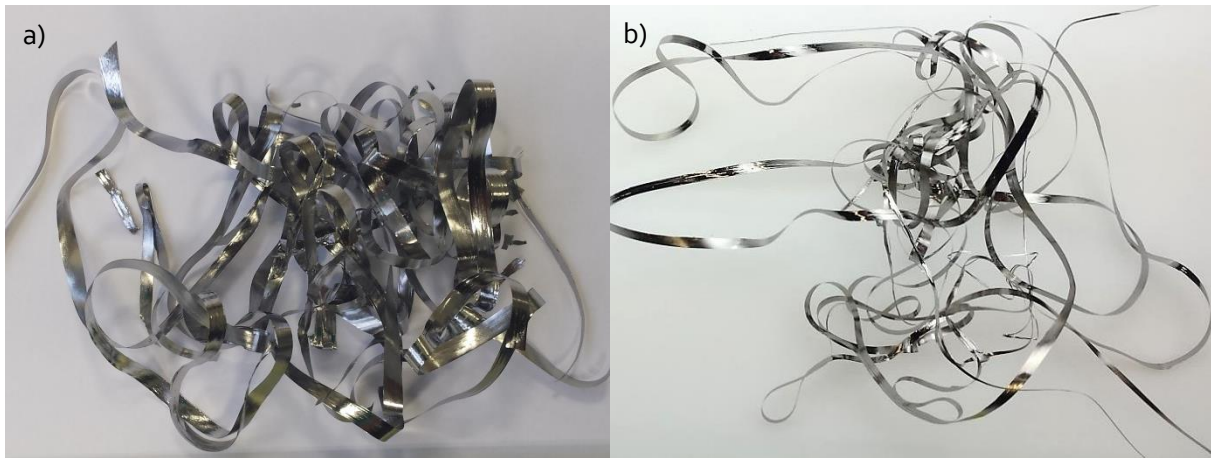


Figure 2. a) Ti70Ni30 and b) Ti67Cu15Ni15Si3 braze ribbons produced by melt spinning.

4.2 Transmission Electron Microscopy (TEM)

Figure 3 shows TEM images of the Ti70Ni30 and Ni67Cu15Ni15Si3 braze ribbons in their initial state after melt spinning. The corresponding selected area diffraction pattern (SADP) is depicted in the upper right corner of each figure.

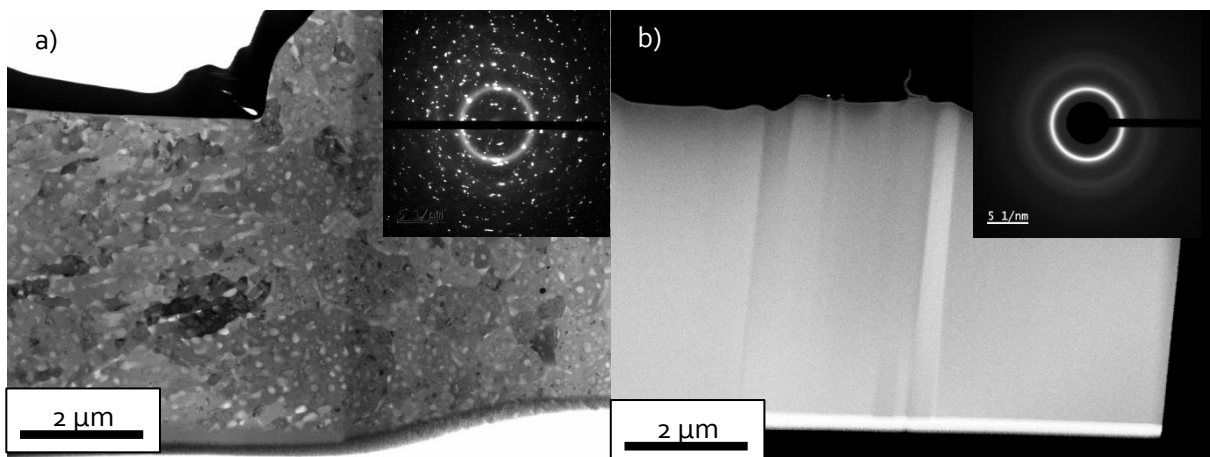


Figure 3. TEM images of the braze ribbons with SADP as insert in the right upper corner. a) Ti70Ni30 b) Ti67Cu15Ni15Si3.

Within the Ti70Ni30 braze ribbon, a grain structure can be found, figure 3a. Grain sizes in the sample are homogeneous and the distribution of grains is uniform. Referring to the corresponding SADP, the bright spots in the image represent a discrete diffraction condition of the sample's crystal structure. Thus, the crystalline structure of the material can be clearly detected. Amorphous areas could not be found. Figure 3b shows the TEM image of the Ti67Cu15Ni15Si3 braze ribbon as well as the corresponding SADP. In the image, the sample is depicted as a grey object without any structure, i.e. no grains can be found in this ribbon. In addition, the corresponding SADP shows no point reflections or clearly distinguishable diffraction rings as well, leading to the assumption that the ribbon has no lattice structure, meaning that the material is fully amorphous.

4.3 Differential Scanning Calorimetry (DSC)

Figure 4 shows the results of the DSC analysis of the Ti70Ni30 braze ribbon. In addition, the image shows the DSC curve of the Ti67Cu15Ni15Si3 ribbon in its initial state as well as after annealing at $T = 860\text{ }^{\circ}\text{C}$ for $t = 10\text{ min}$ in vacuum.

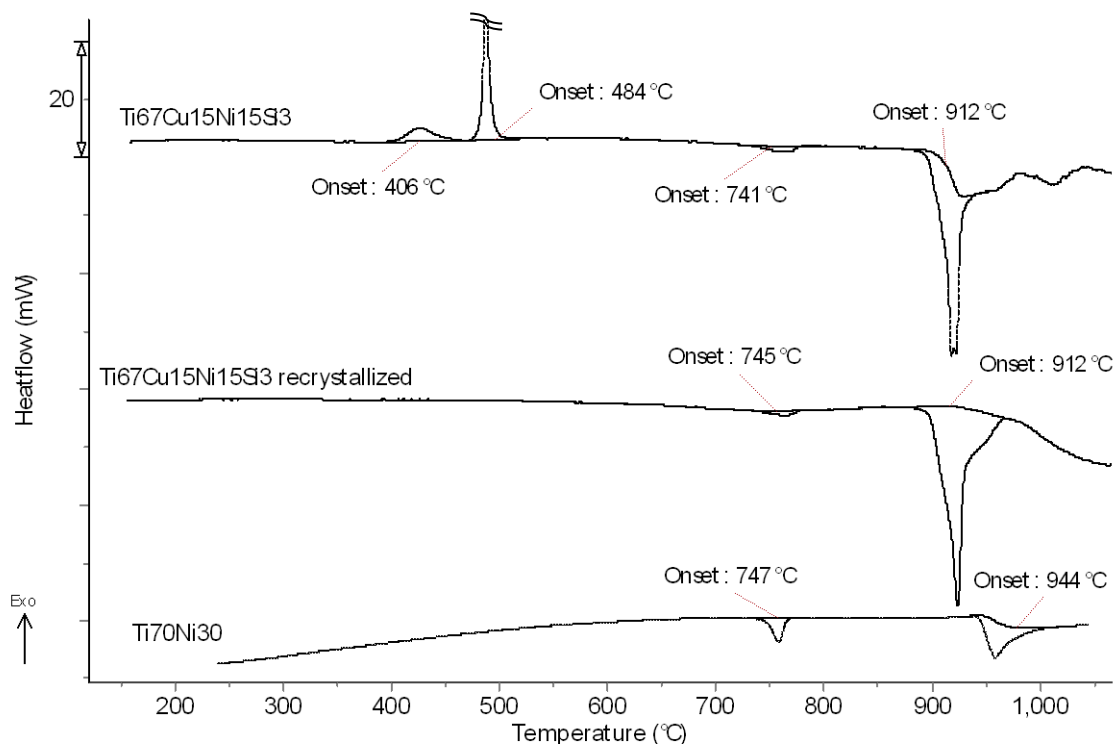


Figure 4.: DSC results of the Ti70Ni30 braze ribbon, the Ti67Cu15Ni15Si3 ribbon in its initial state as well as recrystallized after annealing in vacuum atmosphere at $T = 860\text{ °C}$ for $t = 10\text{ min}$.

The Ti70Ni30 braze ribbon undergoes a phase transition at $T = 747\text{ °C}$, indicated by an endothermic reaction starting at this temperature as shown in figure 4. The binary Ti-Ni phase diagram shows that the initial $\alpha\text{-Ti} + \text{Ti}_2\text{Ni}$ microstructure turns into $\beta\text{-Ti} + \text{Ti}_2\text{Ni}$ at $T = 765\text{ °C}$ [9]. Referring to the DSC analysis, the melting temperature of the alloy is $T_m = 944\text{ °C}$, marked by an endothermic peak in figure 4. Thus, the alloy melts below the austenitization temperature $T_{a/\gamma} = 1,030\text{ °C}$ of the steel 1.2343.

Figure 4 also shows the results of the DSC analysis of the Ti67Cu15Ni15Si3 ribbon in its initial state. While heating the amorphous ribbon up to $T = 1,100\text{ °C}$, the material shows multiple thermic effects. At $T = 406\text{ °C}$, a small exothermic peak can be observed, indicating the start of recrystallization of the ribbon. A further significant exothermic peak can be observed starting at $T = 484\text{ °C}$. The narrow, steep peak marking this reaction in figure 4 indicates a spontaneous, thermally induced “flipping” of the initial amorphous structure of the ribbon into a crystalline structure. Continuing the DSC analysis, a small endothermic peak can be observed at $T = 741\text{ °C}$. This reaction represents a phase transition of the alloy. Due to the complex composition of the ribbon, it is difficult to designate the specific phase reaction that happens at this temperature. The Ti70Ni30 alloy showed an endothermic phase transition at $T = 747\text{ °C}$, in which the mixed phase $\alpha\text{-Ti/Ti}_2\text{Ni}$ transduced to $\beta\text{-Ti} + \text{Ti}_2\text{Ni}$. A similar phase transition can be assumed for Ti67Cu15Ni15Si3, with Si presumably shifting the transition reaction to slightly lower temperatures. Furthermore, the influence of Cu and Si must be taken into account in terms of thermodynamics of this reaction as well as its influence on the probability of the formation of further phases. The melting temperature of the alloy Ti67Cu15Ni15Si3 is $T_m = 912\text{ °C}$, indicated by an endothermic peak of the corresponding graph in figure 4. In comparison to the melting temperature of the Ti70Ni30 braze ribbon at $T_m = 944\text{ °C}$, a reduction in the melting temperature of $\Delta T = 32\text{ K}$ could be achieved by the addition of Cu and Si to the alloy.

To investigate the influence of the amorphous structure on the phase transition temperature of the Ti67Cu15Ni15Si3 ribbon, a further experiment was conducted. A sample of the amorphous braze ribbon was annealed at $T = 860\text{ °C}$ for $t = 10\text{ min}$. Referring to figure 4, the ribbon should fully recrystallize at $T = 486\text{ °C}$. The non-amorphous ribbon was then analyzed via DSC, see figure 4. During DSC analysis, no exothermic reactions, as observed for the amorphous ribbon of same composition, can be found. The experiment validates that the exothermic reactions of the non-annealed Ti67Ni15Ni15Si3 ribbon represents its temperature of recrystallization. Furthermore, the previously annealed ribbon shows a weak endothermic reaction at $T = 745\text{ °C}$, assumably indicating the phase transition of α -Ti to β -Ti, that could be observed for the amorphous braze ribbon as well at slightly lower temperatures. Above $T = 484\text{ °C}$, both ribbons are recrystallized and show the same phase transition temperature and thus have identical thermal properties. The DSC analysis of the previously annealed Ti67Cu15Ni15Si3 braze ribbon shows that it also has a melting temperature of $T_m = 912\text{ °C}$. Thus, the amorphous braze material recrystallizes at temperatures much lower than its melting temperature, causing the material to lose its special properties that come with the amorphous structure.

4.4 Process of brazing

Using the brazing process parameters from chapter 3.4, sound joints with the steel 1.2343 could be realized, using Ti70Ni30 and Ti67Cu15Ni15Si3 braze ribbons. Figure 5 shows scanning electron microscopy (SEM) images of cross sections of brazed joints that were each produced at $T_{\text{brazing}} = 1,010\text{ °C}$.

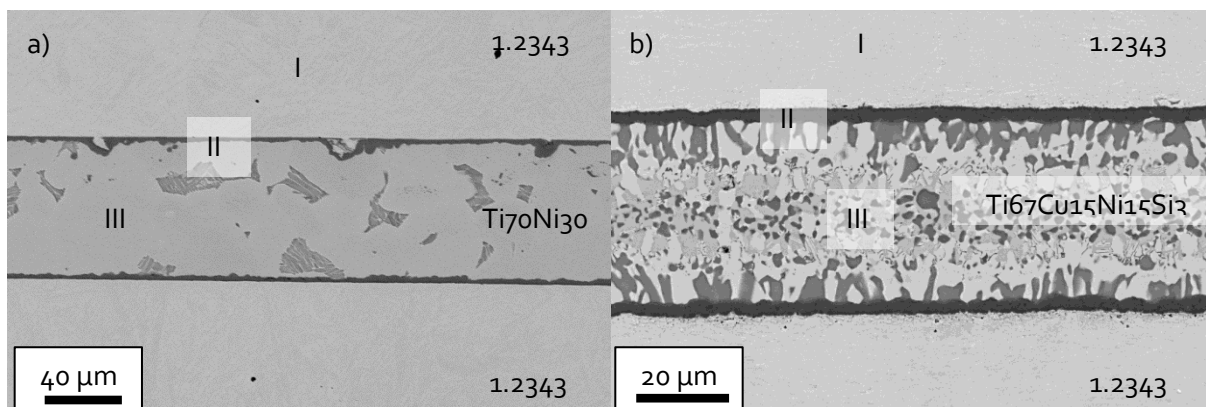


Figure 5. a) SEM images of the joint 1.2343 – Ti70Ni30 – 1.2343, $T_{\text{brazing}} = 1,010\text{ °C}$ b) SEM image of the joint 1.2343 – Ti67Cu15Ni15Si3 – 1.2343, $T_{\text{brazing}} = 1,010\text{ °C}$.

Both joints in figure 5 are characterized by an individual microstructure. The joint that was produced using the Ti70Ni30 braze ribbon, shows a mostly homogeneous microstructure with two phases that can be well distinguished from each other. The interconnection between substrate and brazed seam is established by a Ti-rich reaction layer that is depicted as a dark grey phase between both components marked with “II” in both images. The brazed seam that was produced using the Ti67Cu15Ni15Si3 braze ribbon is characterized by a multiplicity of phases, each distinguished by a different grey tone in figure 5b. The interconnection between braze seam and substrate is also established by a Ti-rich reaction layer at the interface of the joint (“II”). The very complex microstructure of the seam correlates with the complex alloy composition of the braze ribbon, because both joints were produced, using the same process parameters. The effect of the amorphous structure of the Ti67Cu15Ni15Si3 ribbon on the phase formation can also assumed to be nonexistent, because the ribbon fully recrystallizes at temperatures near $T = 484\text{ °C}$, as discussed in section 4.3.

Since the formation of numerous different phases in the brazed seam is difficult to control, the braze alloy Ti67Cu15Ni15Si3 is considered to be critical in terms of precision-relevant aspects.

Additionally, it must be considered that in the brazed seam numerous intermetallics can be found with different thermal expansion coefficients. Thus, a strongly heterogeneous stress zone is created in the joint during cooling at the end of the brazing process, leading to intense residual stresses. With regard to the problems discussed above, the braze alloy Ti70Ni30 is to be preferred, since a much more homogeneous brazed seam is reached during the application of this braze material. A more detailed analysis of the microstructure of the bonds is subject of a paper currently in publication. It is also to be clarified, if during the application of the amorphous braze materials an increased diffusivity of atoms can be observed, whether from the braze material into the substrate or vice versa, compared to the application of non-amorphous braze materials.

4.5 Hardness testing

Brazed joints that were produced using the Ti70Ni30 and Ti67Cu15Ni15Si3 braze ribbons were tested in terms of micro-hardness. For each joint, hardness measurements were conducted at three characteristic positions: $d = 50 \mu\text{m}$ from the interface in the substrate, at the interface and in the center of the brazed seam. These three positions are marked in Roman numerals in figure 5. The results of hardness testing are shown in figure 6.

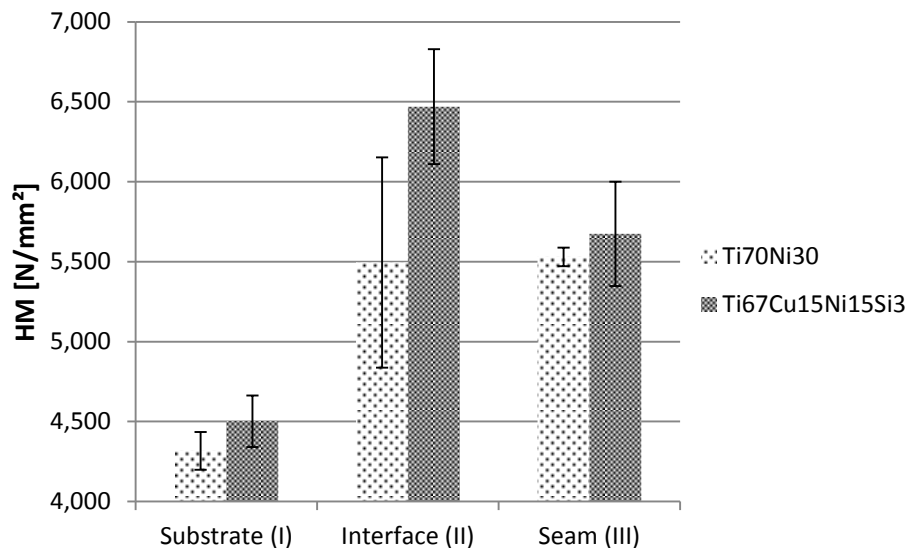


Figure 6. Hardness values of different areas of the joints, as shown in figure 5.

Via hardness testing, the brazed joints can be characterized in terms of their mechanical properties. For the substrate material, hardness values of $HM_I = 4,400 \text{ N/mm}^2$ on average could be measured. The slight deviation of hardness values measured in this region could result from measuring errors or the marginally increased diffusion of atoms from the Ti67Cu15Ni15Si3 braze material into the substrate, compared to the Ti70Ni30 braze material. The hardness value of the substrate serves as a reference for the comparability of the hardness of the phases at the interface and in the brazed seam. The hardness value in the center of both brazed seams is also roughly the same, with approximately $HM_{III} = 5,600 \text{ N/mm}^2$. It is noticeable that the hardness values at position III in the joint produced with the braze material Ti67Cu15Ni15Si3 fluctuate more strongly than in the joint produced with Ti70Ni30. For Ti67Cu15Ni15Si3, the standard deviation of the hardness values at position III is $s_{III} = 326 \text{ N/mm}^2$, whereas for Ti70Ni30 the standard deviation at this point is $s_{III} = 58 \text{ N/mm}^2$. The reason for this difference in standard deviation is the different microstructure of the two joints. A large number of phases is present in the joint produced with the ribbon Ti67Cu15Ni15Si3, see figure 5b. Each of these phases has a different hardness value. During the hardness testing in the center of the brazed seam, no single phase could be tested individually due to the size of the indentation area. As a

result, the hardness value measured for the seam represents an average value of all phases in this region. The joint produced with Ti70Ni30 has a much more homogeneous microstructure, see figure 6a, and thus much more consistent hardness values could be measured in this region.

At the interface of the bond, the relationship between hardness and microstructure is different. At the interface of the joint produced with Ti67Cu15Ni15Si3 hardness values of $HM_{II} = 6,469 \text{ N/mm}^2$ could be measured. The corresponding standard deviation is $s_{II} = 359 \text{ N/mm}^2$. For the joint produced with Ti70Ni30 the hardness value is $HM_{II} = 5,495 \text{ N/mm}^2$, having a standard deviation of $s_{II} = 658 \text{ N/mm}^2$. The thickness of the reaction layer at both brazed joints could be a reason for the different hardness values measured at the interface. The reaction layer of the joint in figure 5a amounts to $d = 2.5 \mu\text{m}$ in thickness. When applying the Ti67Cu15Ni15Si3 braze ribbon, a reaction layer with an average thickness of approximately $d = 3.1 \mu\text{m}$ is established. For micro-hardness testing, the thicker reaction layer of the Ti67Cu15Ni15Si3 joint is easier to detect as the distortive influence of adjacent phases can be estimated to be lower. For this reason, lower hardness values could be measured for the Ti70Ni30 joint, while the corresponding standard deviation increases, as can be seen in figure 6. Figure 7 shows the indents from the micro-hardness testing at the interface of a sample brazed with the Ti67Cu15Ni15Si3 braze ribbon.

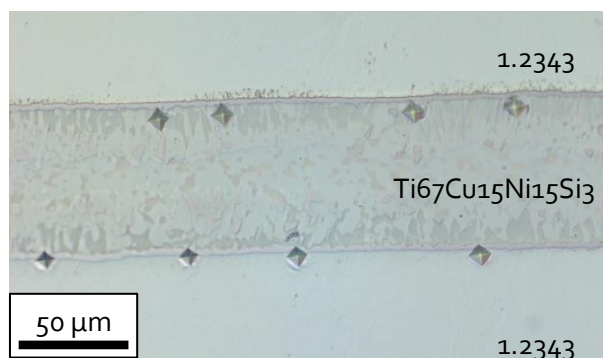


Figure 7. Light microscope image of the joint 1.2343 – Ti67Cu15Ni15Si3 – 1.2343 with indentations from micro-hardness testing at the interface.

Although both investigated joints show high hardness values that are higher than the hardness of the substrate material, subsequent investigations of the indentations via light microscope revealed no evidence of brittle material failure. Therefore, further investigations on the mechanical properties of the compounds are necessary for a more precise characterization.

5. Conclusion

Ti-based braze alloys, having a melting temperature below $T = 1,030 \text{ }^{\circ}\text{C}$ and thus below the austenitization temperature of the steel 1.2343, could be developed and successfully processed into braze ribbons via melt spinning. A fully amorphous ribbon could also be realized. Furthermore, the developed braze ribbons have been successfully used for brazing the steel 1.2343. Investigations on the thermal behavior of the amorphous braze ribbon showed that the amorphous structure disappears when reaching a material-dependent recrystallization temperature which is approximately $\Delta T = 430 \text{ K}$ below the melting temperature T_m of the material. After exceeding the recrystallization temperature, the initially amorphous braze ribbon shares the same melting temperature as the crystalline ribbon of the same composition. First investigations on the mechanical properties of the ribbons showed that solid, non-brittle joints can be produced when applying the braze ribbons developed in this work.

Future studies will aim at a more precise characterization of the brazed joints in terms of mechanical properties, in order to identify and qualify further correlations between brazing process

and brazed joint microstructure with regard to precision-relevant parameters. In addition, the influence of the amorphous structure of a braze material on the diffusion process during brazing shall be investigated.

References

- [1] DIN 857-2:2007-03
- [2] Edmund Bühler GmbH 2011 brochure Bühler Melt-Spinning system (SC-Version) (Hechingen)
- [3] Sahm R; Egry I 1999 *Schmelze, Erstarrung, Grenzflächen. Eine Einführung in die Physik und Technologie flüssiger und fester Metalle* (Braunschweig: Vieweg)
- [4] Uhrig E 2005 *Quasikristalle im System Zink-Magnesium-Seltene-Erden: Materialpräparation und Einkristallzüchtung* (Frankfurt a. M.: Universität Frankfurt a. M.)
- [5] Kalinichenka S 2011 *Rascherstarrte nanokristalline Magnesiumlegierungen für die Wasserstoffspeicherung* (Dresden: TU Dresden)
- [6] Gill P, Moghadam T, Ranjbar B 2010 Differential Scanning Calorimetry Techniques: Applications in Biology and Nanoscience *J. Biomol. Techn.* **21** 167-193
- [7] Hoehne G W H, Hemminger W, Flammersheim H J 1996 *Differential Scanning Calorimetry: An Introduction for Practitioners* (Heidelberg: Springer-Verlag Berlin)
- [8] Hoyer I 2005 *Beitrag zur Entwicklung von Hochtemperaturloten auf Eisenbasis* (Chemnitz: TU Chemnitz)
- [9] ASM International 1992 *Handbook of Ternary Alloy Phase Diagrams* **3** (Ohio: Materials Park)

Acknowledgments

All presented investigations were conducted in the context in the Collaborative Research Centre SFB 1120 “Precision Melt Engineering” at RWTH Aachen University and funded by the German Research Foundation (DFG). For the sponsorship and the support we wish to express our sincere gratitude.